# Chapter 1
# Introduction


**Abstract** This thesis focuses on the fabrication and physical properties study of novel two-dimensional (2D) atomic crystals beyond graphene. In the introduction, we first introduce readers the research background and then review four graphene-like 2D crystal materials, i.e., silicene, germanene, transition-metal dichalcogenides (TMDs), and hexagonal boron nitride (*h*-BN). Lastly, an introduction of research contents and instruments is presented.

**Keywords** Two-dimensional material · Atomic crystal · Graphene · Graphene-like · Van der Waals heterostructure

## 1.1 The Rise and Development of Graphene-Like 2D Crystal Materials

### *1.1.1 From Graphene to Graphene-Like 2D Crystal Materials*

Graphene, a planar monolayer of carbon atoms with a two-dimensional (2D) honeycomb structure, is the first 2D atomic crystal. After its birth by isolation from graphite in 2004, it has become to be the hottest star in material science and attracted tremendous attraction in many different fields in the past ten years [1–3]. Its exotic properties, such as high surface area, high thermal conductivity, extremely high carrier mobility, and quantum Hall effect [4–9], enable potential graphene applications in electronics, photonics, energy generation and storage, and biosensors [10–14]. In order to achieve these promising applications, many preparation methods have been developed to produce few-to-monolayer graphene, such as mechanical and liquid-phase exfoliation, reduction of graphene oxides, chemical vapor deposition, and molecular beam deposition [15–23].

After an intensive study of graphene in the last ten years, "research on simple graphene has already passed its zenith" and "researchers have now started paying more attention to other two-dimensional atomic crystals such as isolated monolayers and few-layer crystals of hexagonal boron nitride (*h*-BN), molybdenum disulfide ($MoS_2$), other dichalcogenides and layered oxides", as claimed by Geim and Grigorieva [24]. Such materials present the entire range of electronic structures,



L. Li, *Fabrication and Physical Properties of Novel Two-dimensional Crystal Materials Beyond Graphene: Germanene, Hafnene and $PtSe_2$*, Springer Theses,
https://doi.org/10.1007/978-981-15-1963-5_1

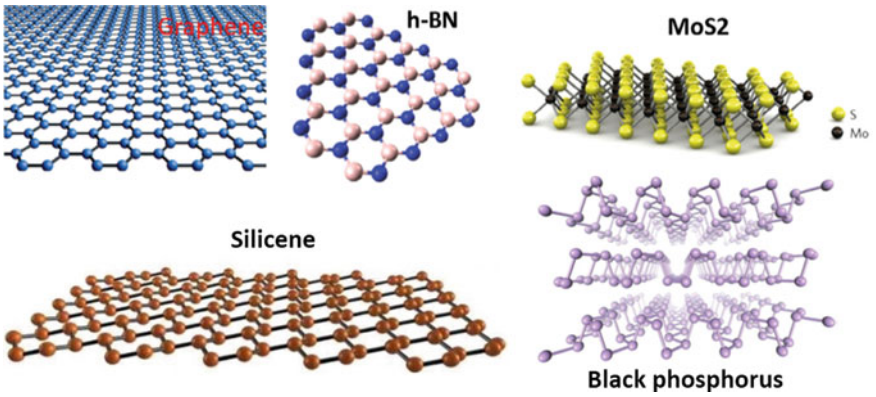


**Fig. 1.1** Graphene and other two-dimensional materials. Reproduced with permission from Ref. [105], © 2014 Elsevier Ltd; [60], © 2015 Springer Nature; [59], © 2014, Springer Nature

from insulator to metal, from semiconductor to semi-metal and display many interesting properties, such as superconductivity, charge density wave, and topological insulator effect [25–46]. Moreover, graphene-like 2D buckled honeycomb structures have been attracting attention. These include silicene and germanene, the silicon- and germanium-based counterparts of graphene, which have been prepared experimentally after theoretical predictions and display atomic and electronic characteristics similar to graphene [47–54]. Based on their distinct properties, these 2D materials, as shown in Fig. 1.1, exhibit various application potentials on electronics, optoelectronics, catalysis, chemical sensors, and lithium-ion batteries [28–30, 39, 40, 42, 55–60].

### *1.1.2 Synthesis and Characterization*

In general, all the methods employed for the synthesis and characterization of graphene could also be used effectively in the case of other 2D crystals. Thus, that is, single- and few-layer graphene-like 2D atomic crystals can be prepared by both physical and chemical methods. Mechanical exfoliation (scotch-tape technique), the first successful method for generating graphene, has already been used with other layered materials such as $MoS_2$ and $NbSe_2$ [61]. Liquid-phase cleavage assisted by ultrasonication has been employed to prepare many layered inorganic layered materials [62, 63]. Molecular beam epitaxial (MBE) has been successfully applied to the production of silicene and germanene [49, 53, 54]. Chemical methods include chemical synthesis, chemical vapor deposition (CVD), and atomic layer deposition (ALD). In particular, CVD is the most popular method for preparing large-scale 2D materials [35, 37, 64–68].

Single- and few-layer 2D materials are generally characterized by transmission electron microscope (TEM), scanning electron microscope (SEM), and scanning tunneling microscope (STM). Moreover, Atomic force microscope (AFM) has been demonstrated to be a powerful technique to determine layer thickness with a precision of 5%. Layer-dependent vibrational information can be obtained by Raman spectroscopy. X-ray diffraction can be employed to determine unit cell structure, the film thickness, and chemical constituents. Therefore, characterization of 2D materials is performed by a variety of microscopic and spectroscopic techniques.

## 1.2 Silicene and Germanene

### *1.2.1 Theoretical Investigations*

The discovery and success of graphene have sparked new explorations on graphene-like films composed of other group-IV elements, such as so-called silicene and germanene, which are considered as Si- and Ge-based 2D counterparts of graphene. The planar honeycomb structure of graphene stems from the equivalently covalent bonds of carbon atoms formed by the fully $sp^2$-hybridized state. However, unlike graphene, in the case of Si and Ge, the $sp^3$-hybridized state is more stable than the planar $sp^2$-hybridized state. So that, silicene and germanene tend to form a mixed $sp^2$–$sp^3$ hybridized state with a buckled honeycomb structure rather than a planar one. That is also why there are no layered phases in bulk Si and Ge, in contrast to graphite (bulk C). Therefore, we cannot produce silicene or germanene sheets by micromechanical exfoliation of their bulk counterparts. However, we can still construct silicene and germanene structures by employing theoretical approaches. Actually, before exfoliation of graphene, first-principles calculations were performed to predict the most stable configurations for group-IV single sheets [69]. In contrast to the planar honeycomb lattice of graphene, Si and Ge monolayers can be stable with a nonplanar configuration, i.e., buckled honeycomb structure.

The first-principles calculations showed that the planar (PL) and high-buckled (HB) atomic structures of single-layer Si and Ge sheets are unstable, but the low-buckled (LB) honeycomb structures, as displayed in Fig. 1.2, can be stable, where the perpendicular distance between top and bottom Si (Ge) sublayers is $\Delta \approx 0.44$ Å (0.64 Å), forming the mixed $sp^2$–$sp^3$ hybridized orbitals [70]. In the LB honeycomb structure of silicene (germanene), the lattice constant and nearest-neighbor atomic distance are 3.86 Å (4.02 Å) and 2.28 Å (2.42 Å), respectively. In contrast to the C–C distance (1.42 Å) in graphene, much larger Si–Si and Ge–Ge atomic distances severely decrease the electronic overlaps of $\pi$–$\pi$ bonds.

S. Cahangirov et al. calculated the electronic energy band spectra of Si and Ge for HB, PL and LB configurations and corresponding density of states (DOS) for LB structures [70]. As shown in Fig. 1.3, both HB Si and Ge are metallic. Similar to graphene, $\pi$ and $\pi^*$ bands of PL and LB silicene cross at the K point in the Fermi

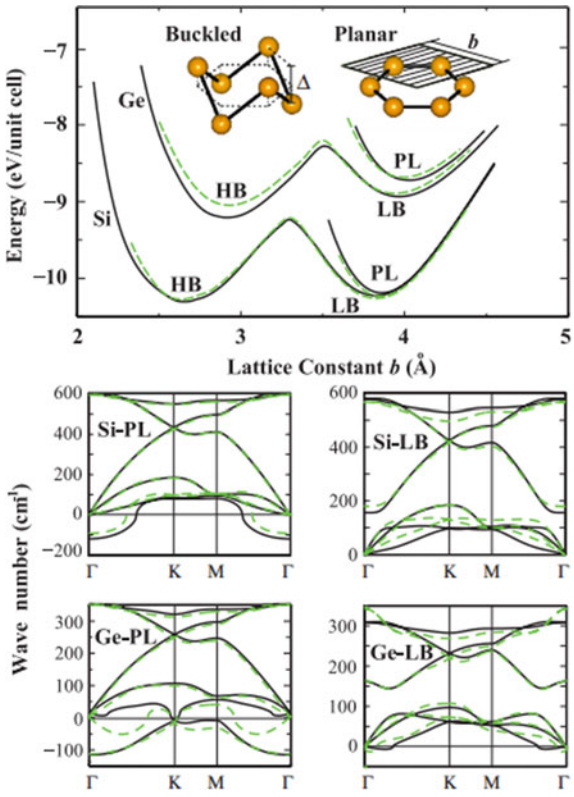


**Fig. 1.2** Energy versus hexagonal lattice constant (upper panel) and phonon dispersion curves (lower panels) of 2D Si and Ge are calculated for various honeycomb structures. Reprinted with permission from Ref. [70], © 2009 APS

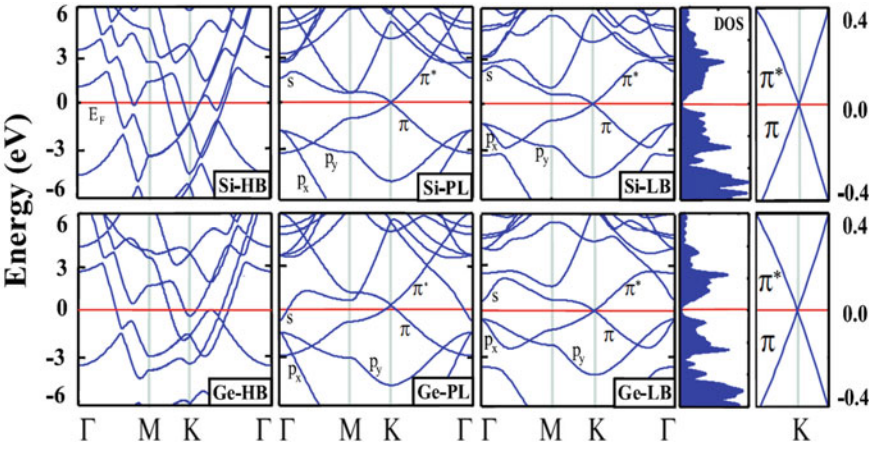


**Fig. 1.3** Band structures of Si and Ge are calculated for high-buckled (HB), planar (PL), and low-buckled (LB) structures. For LB structure the density of states (DOS) is also presented. Reproduced with permission from Ref. [70], © 2009 APS

level (EF) and thus they are semimetallic. Planar Ge structure is metallic due to a low density of s-like states crossing the EF. In contrast, LB structure of Ge shows semimetallic behavior with linear π and π* bands crossing at K point in the EF. This behavior of bands is attributed to a mass-less Dirac fermion character of the charge carriers.

### *1.2.2 Experimental Explorations*

Theoretical investigations demonstrated that silicene (germanene) is a metastable structure, with 0.79 eV/atom (0.67 eV/atom) higher energy compared to bulk Si (Ge) structure. It suggests thickness-controllable deposition technique is preferred for silicene and germanene growth, such as molecular beam epitaxy and low-temperature atomic layer deposition, in order to avoid the formation of three-dimensional structures. It should be mentioned that there is not yet any report on the successful preparation of germanene prior to our research (the early explorations of germanene growth are exhibited in Sect. 2.1.2). Therefore, we will only review the experimental investigations on the growth of silicene as follows.

Experimental explorations of silicene began with silver (Ag) surfaces, as Si/Ag system tends to phase separation due to the very low solubility of Si in bulk Ag.

First, silicon nanoribbons were obtained by Si deposition onto Ag(110) surface under ultrahigh vacuum [71–73]. STM measurements revealed Si honeycomb structures inside the nanoribbon, as shown in Fig. 1.4. Correspondingly, DFT calculations showed that Si atoms have a tendency toward honeycomb arrangement on the Ag surfaces. Moreover, the simulated STM images displayed a buckled honeycomb structure, in agreement with the experimental observations. This is the first evidence of the existence of silicene.

In 2010, Lalmi, B. et al. claimed that they succeeded in preparing a continuous, two-dimensional sheet of silicene on Ag(111) surface [74]. However, the Si–Si atomic distance in the honeycomb structure is only 0.19 nm directly measured

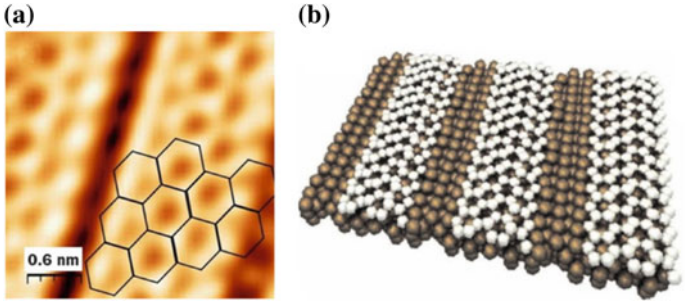


**Fig. 1.4** **a** High-resolution STM image and **b** calculated atomic structure of silicon nanoribbons. Reprinted from Ref. [71], © 2010 AIP Publishing; [72], © 2010 AIP Publishing

from their STM images, which is too much smaller than the calculated value (0.22–0.24 nm). Le Lay et al. argued that the observed honeycomb lattice did not correspond to a silicene layer but instead to the bare Ag(111) surface with a contrast inversion [75]. In subsequent studies of the growth of silicene on Ag(111) surface, the $4 \times 4$ and $(\sqrt{13} \times \sqrt{13})$R13.9° superstructures have been found [76] and a $(\sqrt{7} \times \sqrt{7})$R19.1° structure has been predicted [77], as shown in Fig. 1.5. Feng et al. also found the $4 \times 4$ and $(2\sqrt{3} \times 2\sqrt{3})$R30° superstructures, although they proposed different theoretical structural models [49]. More importantly, they revealed a new superlattice $(\sqrt{3} \times \sqrt{3})$R30°, as illustrated in Fig. 1.6. They constructed the following atomic structure: two Si atoms in a honeycomb ring are buckled upward and one atom is buckled downward, forming a tri-sublayer structure. They also studied the dI/dV spectra of silicene and found the Dirac point of silicene at around $0.52 \pm 0.02$ eV.

Our group has been involved in the research of graphene and graphene-like 2D materials for years. Recently we successfully prepared silicene sheets on an Ir(111) surface by MBE [53]. STM and LEED observations, as presented in Fig. 1.7, revealed that the silicene layer possesses a $(\sqrt{7} \times \sqrt{7})$ superstructure with respect to the underlying Ir(111) surface, which agrees well with a low-buckled atomistic model of silicene generated by DFT calculations. Importantly, the calculated electron localization function revealed 2D continuity of silicene layer on the Ir(111) substrate. This work provides a method to fabricate high-quality silicene and an explanation for the formation of the buckled silicene sheet.

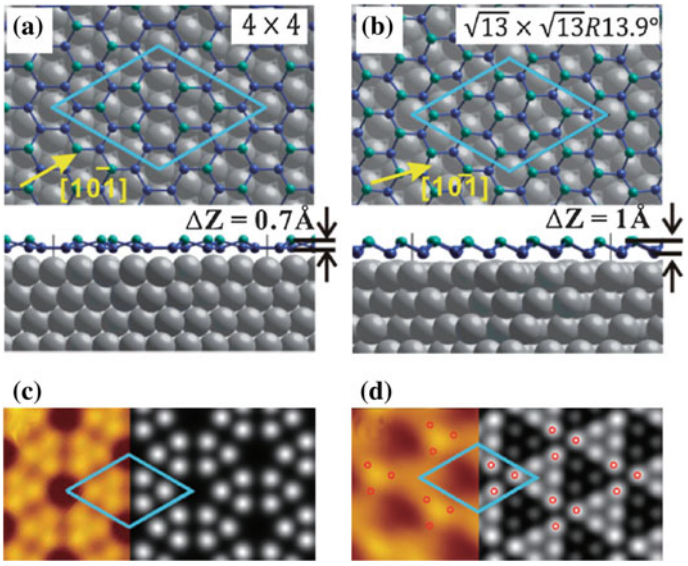


**Fig. 1.5** Optimized structure models and simulated STM images of **a**, **c** $4 \times 4$ and **b**, **d** $(\sqrt{13} \times \sqrt{13})$R13.9° silicene on Ag(111). Reproduced with permission from Ref. [76], © 2012 The Japan Society of Applied Physics

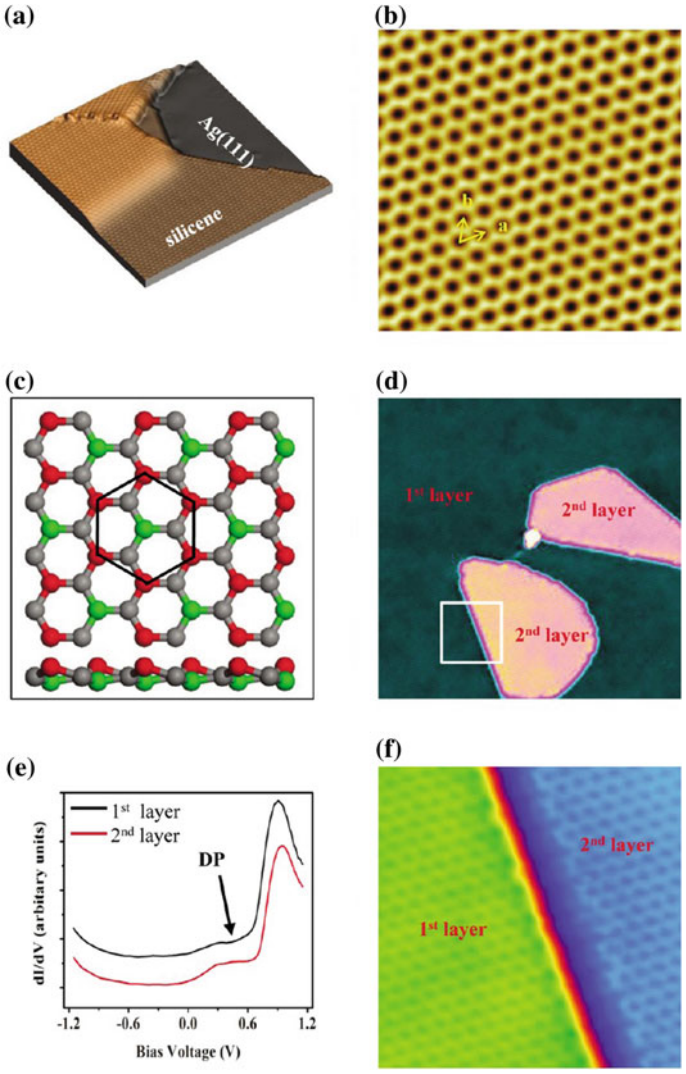


**Fig. 1.6** STM observations, schematic model, and dI/dV spectroscopy of ($\sqrt{3} \times \sqrt{3}$) superstructure of silicene on Ag(111). Reprinted with permission from Ref. [49], © 2012 ACS

Besides the metal substrates mentioned above, there is a report on the growth of silicene on $ZrB_2$ surface supported on a Si(111) substrate [50], as shown in Fig. 1.8. Instead of directly depositing silicene, the researchers found a (2 × 2) reconstructed structure on the $ZrB_2(0001)$ surface, which was considered to be separated from the underlying Si(111) substrate and assigned to the ($\sqrt{3} \times \sqrt{3}$) superstructure of silicene layer. They characterized and studied its atomic structures and electronic properties by performing STM, XPS, ARPES, and ab initio calculations.

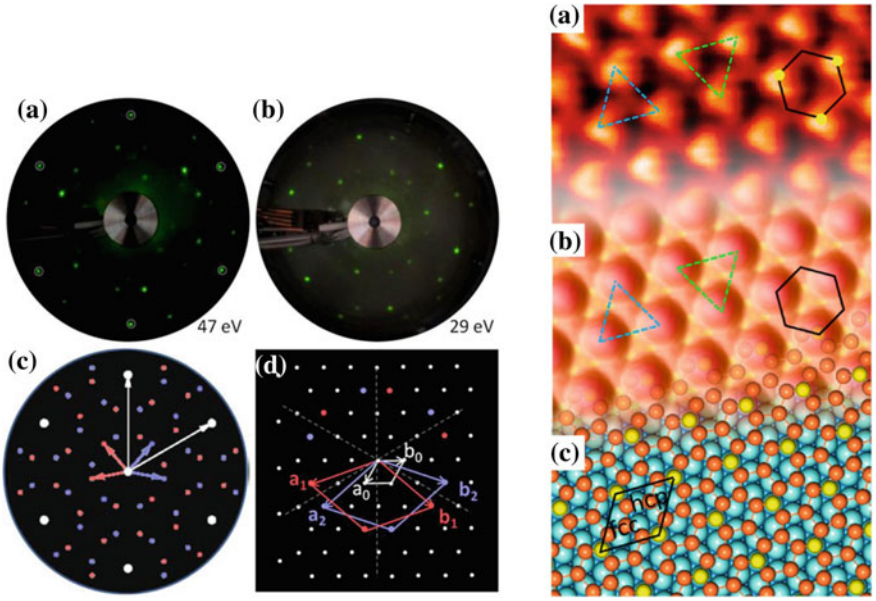


**Fig. 1.7** Left: **a**, **b** LEED patterns and **c**, **d** theoretical LEED patterns of ($\sqrt{7} \times \sqrt{7}$) superstructure of silicene. Right: **a** STM image, **b** simulated STM image, and **c** calculated atomic structure of ($\sqrt{7} \times \sqrt{7}$) superstructure of silicene on Ir(111). Reproduced with permission from Ref. [53], © 2013 ACS

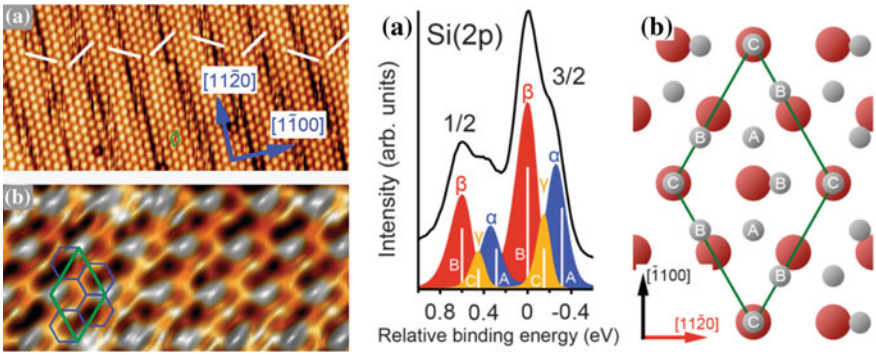


**Fig. 1.8** High-resolution STM images, XPS measurement, and atomic model of Si (2 × 2) reconstructed structure on $ZrB_2$(0001) surface. Reproduced from Ref. [50]

## 1.3 Transition Metal Dichalcogenides

### *1.3.1 The Rise of TMDs*

In the past ten years, the intensive studies of graphene and the rapid progress in the methodology developed in preparing ultrathin films have sparked new explorations and discoveries of novel 2D crystal materials beyond graphene. In particular, layered transition metal dichalcogenides (TMDs) have attracted considerable attention because of their diverse physical properties and a variety of potential applications [30, 58]. It is well known that graphene, on the one hand, is chemically inert and can only be functionalized by introducing desired molecules, which in turn will influence its novel properties. On the other hand, graphene has no bandgap, which considerably weakens and hinders its technological applications in the semiconductor industry. Band gaps can be opened with experimental methods, such as chemical functionalization, fabrication of graphene nanostructures, but these methods increase the process difficulty and result in the loss of electron mobility.

In contrast, TMDs show a wide range of physical and chemical properties, with their electronic structures ranging from insulators, semiconductors, to semimetals, and pure metals. Some bulk TMDs materials show low-temperature phenomena, such as charge density wave (CDW) and superconductivity [25, 31]. The exfoliated few- or single-layer TMDs nanosheets exhibit properties distinct from that in graphene [28, 29, 32], which could complement and enhance the application potentials of graphene. For example, several monolayer TMDs possess sizable bandgaps around 1–2 eV, which enable them to be promising optoelectronic devices [26, 30, 40, 55, 56]. The versatile properties of TMDs offer a platform for both fundamental research and technological applications.

### *1.3.2 Structural Properties of TMDs*

The formula of TMDs materials is $MX_2$, where M is one of transition metal elements of groups 4–10 (such as Hf, Ta, Mo, W, and Pt), and X is a chalcogen (S, Se or Te). These layered crystals adopt sandwich-like structures with the form X-M-X, where a sublayer of metal atoms is sandwiched by two hexagonally packed planes of chalcogen atoms. An individual $MX_2$ monolayer is defined by three sublayers of atoms (X-M-X) in which the M and X atoms are bonded covalently. Adjacent monolayers are weakly held by Van der Waals forces to form 3D stacked crystal, as depicted in Fig. 1.9. Bulk TMD crystals possess three polymorphs depending on stacking orders and the coordination of metal atoms by the chalcogens. In both 2H and 3R phases, the metal coordination is trigonal prismatic (honeycombs), while the coordination in 1T-$MX_2$ is octahedral (centered honeycombs). Here, the digit indicates the number of X-M-X layers in each stacking unit cell, and the letters represent the types of symmetry: hexagonal (H), rhombohedral (R), and trigonal (T). For instance, bulk $MoS_2$

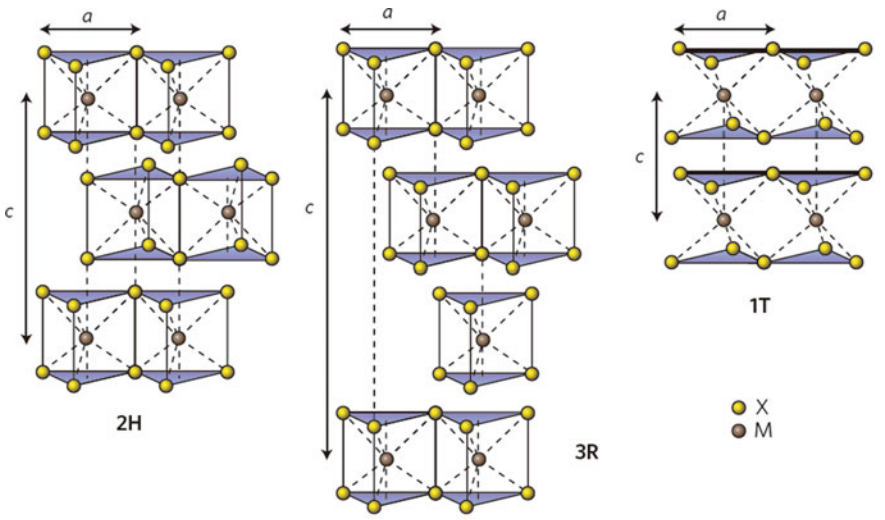


**Fig. 1.9** Schematics of the structural polytypes of layered TMDs materials. Reproduced with permission from Ref. [30], © 2012 Springer Nature

is a prototypical TMD commonly found in the "2H phase", in which each $MoS_2$ unit cell contains two layers of S-Mo-S sandwiches with a hexagonal symmetry in the vertical projection.

Note that monolayer TMDs show only two polytypes: trigonal prismatic and octahedral phases, generally referred to as 1H and 1T $MX_2$, respectively, as depicted in Fig. 1.10.

## *1.3.3 Electronic Properties of TMDs*

### 1.3.3.1 Electronic Properties of Bulk TMDs

Depending on the coordination and oxidation state of the metal atoms, layered TMDs can be semiconducting (e.g. M = Mo, W) or metallic (e.g. M = Ta, Nb). As shown in Fig. 1.11, a simple model for ideal coordination is exhibited to explain the diverse electronic properties of TMDs crystals. In both 1H and 1T phases, the non-bonding d orbitals of the TMDs are located within the bandgap of bonding (σ) and anti-bonding states (σ*) in group 4, 5, 6, 7 and 10 TMDs. According to ligand field theory, Octahedrally coordinated transition metal centers of TMDs form two non-bonding d orbitals, $d_{yz,xz,xy}$ (bottom) and $d_{z2,\ x2-y2}$ (top), while transition metals with trigonal prismatic coordination exhibit three d orbitals, $d_{z2}$, $d_{x2-y2,xy,}$ and $d_{xz,yz}$ (from bottom to top). The diversity of electronic properties of TMDs arises from the progressive filling of the non-bonding d orbitals from group 4 to group 10 species. When an

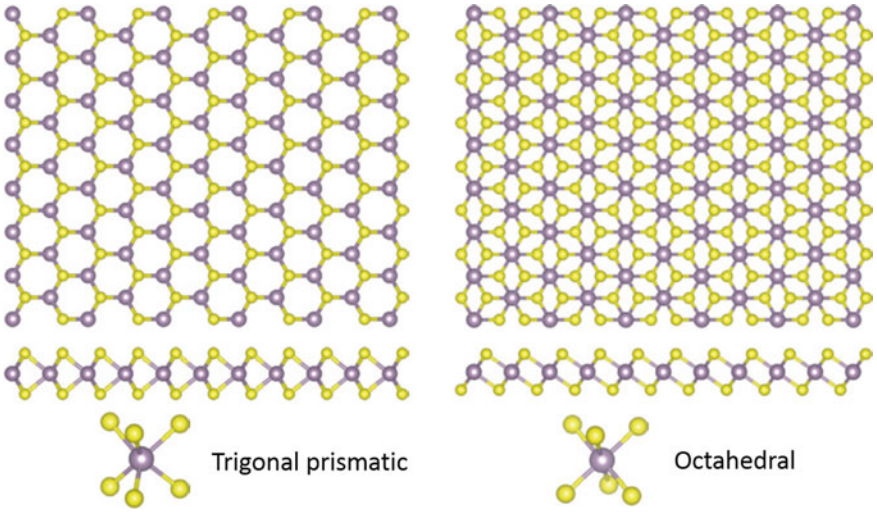


**Fig. 1.10** Structural models of single-layer TMDs with trigonal prismatic and octahedral coordination. Reprinted with permission from Ref. [58], © 2013 Springer Nature

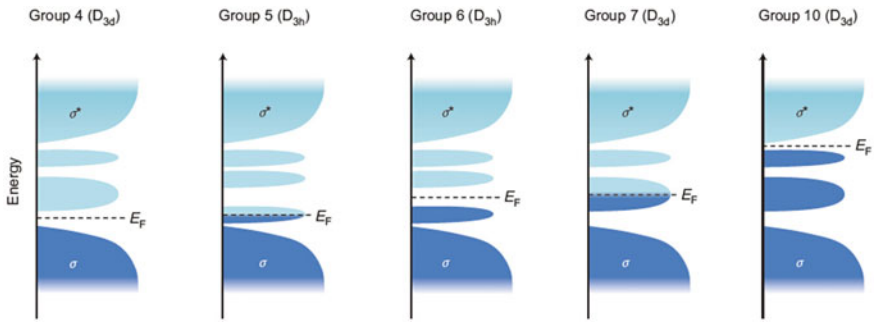


**Fig. 1.11** Schematic illustration showing progressive filling of d orbitals of TMDs. Reproduced with permission from Ref. [58], © 2013 Springer Nature

orbital is partially filled, as in the case of 2H-$NbSe_2$ and 1T-$ReS_2$, the Fermi level is within the band, and the compounds exhibit a metallic character. When an orbital is fully filled, such as in 1T-$HfS_2$, 2H-$MoS_2$, and 1T-$PtS_2$, the Fermi level is located in the energy gap, and a semiconducting character is observed.

### 1.3.3.2 Band Structures of Single-Layer TMDs

Due to the effect of quantum confinement and changes in interlayer coupling, single-layer TMDs prepared by deposition or isolation go through considerable changes in

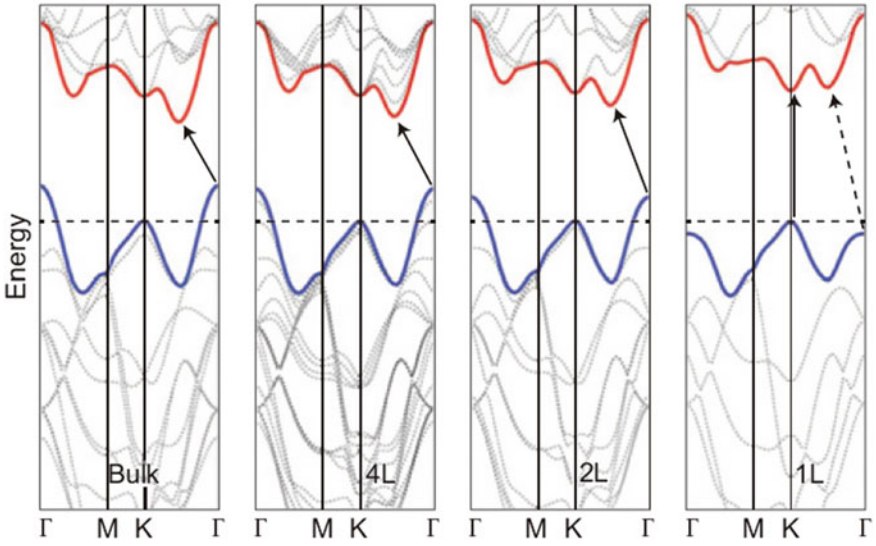


**Fig. 1.12** Band structures of bulk and few- to mono-layer $MoS_2$. Reprinted with permission from Ref. [55], © 2010 ACS

band structures compared to their bulk counterparts. For example, the band structures of bulk, few- and mono-layer $MoS_2$ calculated from first principles are exhibited in Fig. 1.12. At the Γ point, the bandgap is indirect for the bulk material but gradually shifts to be direct for the monolayer. This indirect-to-direct bandgap transition with layer number is due to quantum confinement and the resulting change in hybridization between $p_z$ orbitals on S atoms and d orbitals on Mo atoms. Several studies have confirmed a similar band transition for $MoSe_2$, $WS_2$, and $WSe_2$, which accounts for the enhanced photoluminescence in monolayers of $MoS_2$, $MoSe_2$, $WS_2$, and $WSe_2$, in contrast to only weak emission observed in multilayered forms [26, 55, 56, 78, 79]. The transition to a direct bandgap in the monolayer form enhances the absorption and emission efficiency of photons and thus has important applications for the photonics, optoelectronics, and sensing.

### *1.3.4 Synthesis of TMDs*

Preparation of materials is the prerequisite for fundamental research, and the essential step toward translating their unique properties into applications. Until now, many methods have been employed to prepare ultrathin TMDs materials. The top-down

methods, which rely on the exfoliation of layered bulk crystals, include the mechanical cleavage method, liquid-phase exfoliation by direct sonication, chemical Li-intercalation and exfoliation, and laser thinning technique. Examples of bottom-up approaches are CVD growth and wet chemical synthesis.

#### 1.3.4.1 Top-Down Preparation

Mechanical exfoliation, as shown in Fig. 1.13, is the original technique developed for graphene [80]. It remains the best method for preparing high-purity atomically thin flakes of TMDs peeled from their layered TMD bulks with a view to investigating their inherent physical properties and fabrication of individual devices [61]. However, this method is not scalable and cannot allow precise control of film thickness and size. Therefore, this method cannot be used for mass production in industrial applications.

Liquid-phase exfoliation has been developed to obtain large quantities of exfoliated ultrathin flakes [62, 63, 81–84], which involves dissolution and exfoliation of TMDs powders by direct sonication in commonly used solvents such as dimethylformamide and N-methyl-2-pyrrolidone. One of the disadvantages of liquid exfoliation is the difficulty in preparing monolayer TMD sheets and maintaining the lateral size of exfoliated nanosheets. Ultrasonic-promoted hydration of lithium-intercalated compounds, as illustrated in Fig. 1.14, is another effective method for mass production of fully exfoliated TMDs layers. This approach utilizes a solution of a lithium-containing compound such as n-butyllithium to achieve intercalation of lithium ions between the layers and thus rapidly separates them into single layers. Although the yield of the lithium intercalation method for obtaining single-layer TMDs is nearly 100%, some challenges remain. The lithium intercalation must be carefully controlled to obtain complete exfoliation instead of the formation of metallic compounds, such as $Li_2S$. Otherwise, the resulting exfoliated material differs structurally and electronically from the bulk material due to the charge transfer between TMDs and alkali ions.

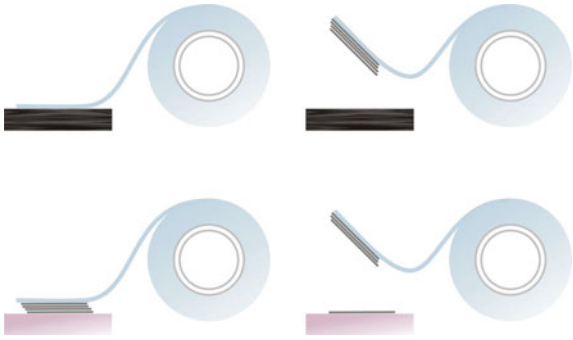

**Fig. 1.13** Illustrations of the "Scotch-tape" method of producing graphene. Reproduced with permission from Ref. [80], © 2011 APS

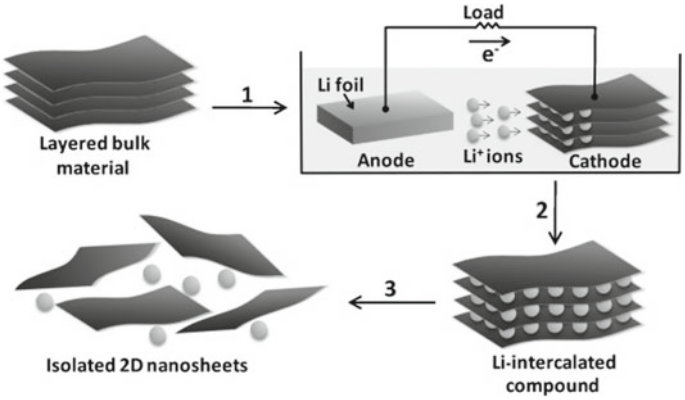


**Fig. 1.14** Electrochemical lithiation process for the fabrication of 2D nanosheets from the layered bulk material. Reproduced with permission from Ref. [82], © 2011 Wiley

### 1.3.4.2 Bottom-up Synthesis

Reliably synthesizing high-quality and large-area ultrathin films is an essential step for applications in electronics and optoelectronics. For example, chemical vapor deposition of graphene on copper foils, as a significant breakthrough in the preparation of large-area graphene, has enabled large-scale device fabrication. Various CVD and CVD-related methods have been developed for growing atomically thin TMDs films [65, 66, 85, 86], as shown in Fig. 1.15, which include three strategies summarized as follows. (I) vaporization of metal and chalcogen precursors and their decomposition, followed by deposition of the resulting TMDs on a substrate, (II)

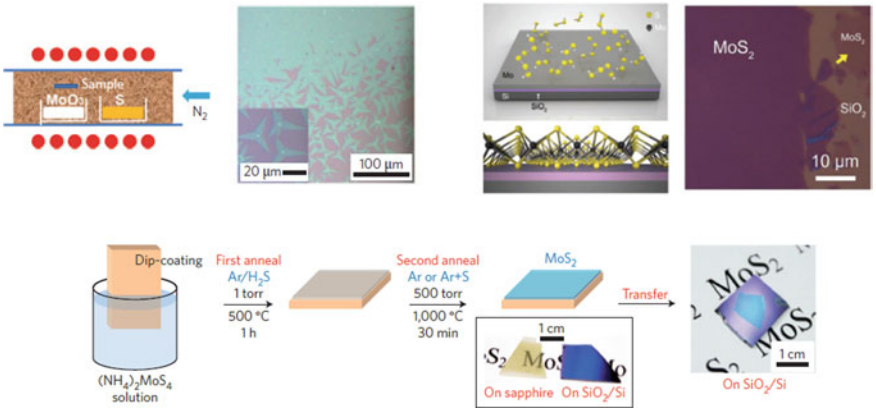


**Fig. 1.15** Schematics of CVD methods for synthesizing $MoS_2$. Reprinted with permission from Ref. [85], © 2012 Wiley; [66], © 2012 Wiley; [65], © 2012 ACS

direct sulfurization of the pre-deposited metal film, and (III) conversion of transition metal oxide (such as $MO_3$) to TMDs ($MX_2$) by sulfurization or selenization.

Besides CVD methods, chemical syntheses of $WS_2$, $MoS_2$, $WSe_2$, and $MoSe_2$ have been demonstrated using hydrothermal synthesis [87–90].

### *1.3.5 Applications of TMDs*

The unique electronic properties of TMDs, especially semiconducting TMDs enable them to have many significant applications for electronics, optoelectronics, energy storage, photovoltaic cells, and photoelectric detection, as will be discussed in more detail below.

#### 1.3.5.1 Electronics

One of the most extensive and important applications of semiconductors is the fabrication of digital circuit transistors. Nowadays, the size of silicon-based field-effect transistors (FETs) has approached its physical limit, motivating people to explore new alternative materials. Digital logic transistors require the properties of high charge carrier mobility, a large on/off current ratio, high conductivity, and low off-state conductivity. Graphene has aroused intense interest due to its two-dimensional characteristics and ultra-high electron mobility [13, 91–93]. However, the lack of energy gap means that the transistor made of graphene cannot achieve low off-state current and thus brings about energy consumption, nor can it effectively control switching with high on/off ratios. Now more and more attention has been paid to ultra-thin semiconducting TMDs, as displayed in Fig. 1.16. As promising field-effect transistor channel materials, TMDs show stable structures free of surface dangling bonds and comparable mobility to those of Si. Their atomic-scale thickness combined with the bandgaps in the range of 1–2 eV enables large on/off switching ratios, a high degree of immunity to short channel effects and thus a considerable reduction in power dissipation [57, 94, 95].

#### 1.3.5.2 Optoelectronics

The electronic band structures of semiconductors play an essential role in optical absorption and emission. For indirect-bandgap semiconductors, they need an additional process of phonon absorption or emission to satisfy the momentum conservation, thus reducing the efficiency of photon absorption and emission. In contrast, many TMDs monolayers, such as $MX_2$ (M = Mo, W, X = Se, Te), possess direct semiconducting bandgaps, in which photons with energy larger than the bandgap width can be readily absorbed and emitted. In addition, because of their sub-nanoscale thinness and processability, they have sparked considerable interest in a wide range

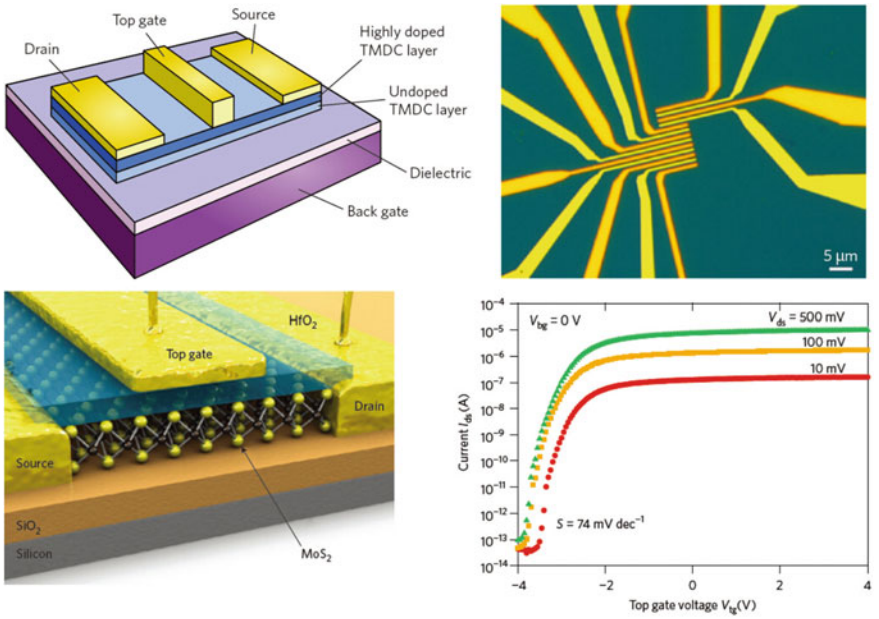


**Fig. 1.16** Schematic illustrations of TMDs-based transistors. Reprinted with permission from Ref. [30], © 2012 Springer Nature; [57], © 2011 Springer Nature

of potential applications for flexible and transparent optoelectronic devices [27, 96], as shown in Fig. 1.17.

#### 1.3.5.3 Light Emission

Light emission can be classified into photoluminescence (PL) and electroluminescence (EL). PL is light emission from a material after the absorption of photons (electromagnetic radiation). It is initiated by photoexcitation (i.e., photons that excite electrons to a higher energy level in an atom). Following excitation, various relaxation processes typically occur in which other photons are re-radiated. PL process is observed in monolayer $MoS_2$, which has a direct bandgap, and the photoluminescent efficiency is demonstrated to be much higher than those of bilayer and bulk $MoS_2$, both of which are indirect-bandgap semiconductors [55, 56]. EL is an optical phenomenon and electrical phenomenon in which a material emits light in response to the passage of an electric current or to a strong electric field. It is the result of radiative recombination of electrons and holes in a material, usually a semiconductor. The excited electrons release their energy as photons-light [97, 98]. In semiconductors with direct band gaps, the combination of electrons and holes and photonic radiation occur more efficiently than in indirect bandgap semiconductors. So the

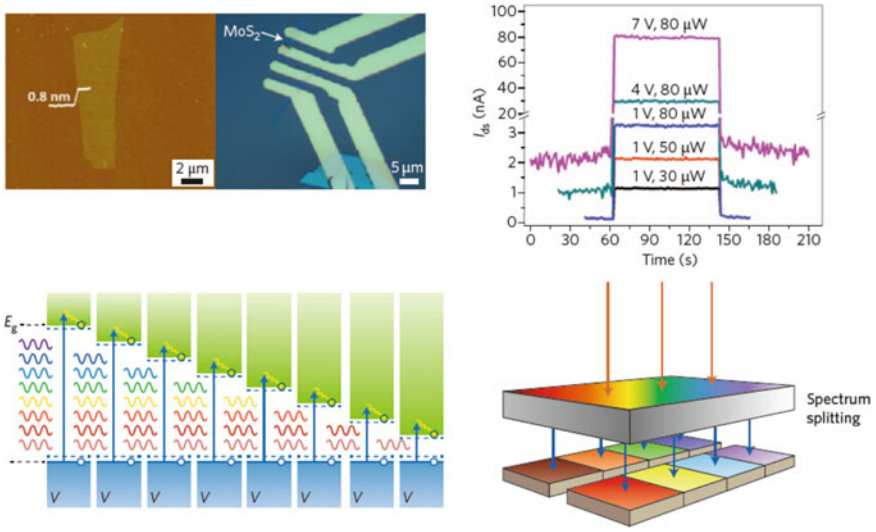


**Fig. 1.17** Current and proposed TMDs optoelectronic devices. Reproduced with permission from Ref. [27], © 2011 ACS; [96], © 2012 Springer Nature

direct bandgaps of monolayer semiconducting TMDs make them the promising light emission materials in flexible optoelectronic devices.

## 1.4 *h*-BN and Other Graphene-Like 2D Materials

Bulk *h*-BN, called "white graphite", has a similar layered structure as graphite with the exception that the basal planes in *h*-BN are vertically aligned to each other, with the electron-deficient B atoms in one layer lying over and above the electron-rich N atoms in adjacent layers, as illustrated in Fig. 1.18. For graphite, however, the adjacent layers are stacked offset, and alternating C atoms lie above and beneath the center of the honeycomb structures. Both bulk *h*-BN and graphite exhibit very similar lattice constants and interlayer distances. Due to their close structural similarity, single-layer *h*-BN can thus be regarded as a structural and isoelectronic analog of graphene, composed of alternating boron and nitrogen atoms in a honeycomb arrangement. It can be obtained by replacing C–C bond with B–N bond in graphene [99, 100].

Although *h*-BN and graphene have similar structures, their electronic properties are strikingly distinct. The pristine *h*-BN sheets are intrinsically insulators or wide band-gap semiconductors (approximately 5.9 eV) [101], in contrast to semi-metallic graphene. Because of its excellent electrical insulation property, *h*-BN has been applied as a charge leakage barrier layer for use in electronic equipments. On the other hand, 2D *h*-BN has many other excellent properties. For example, *h*-BN has

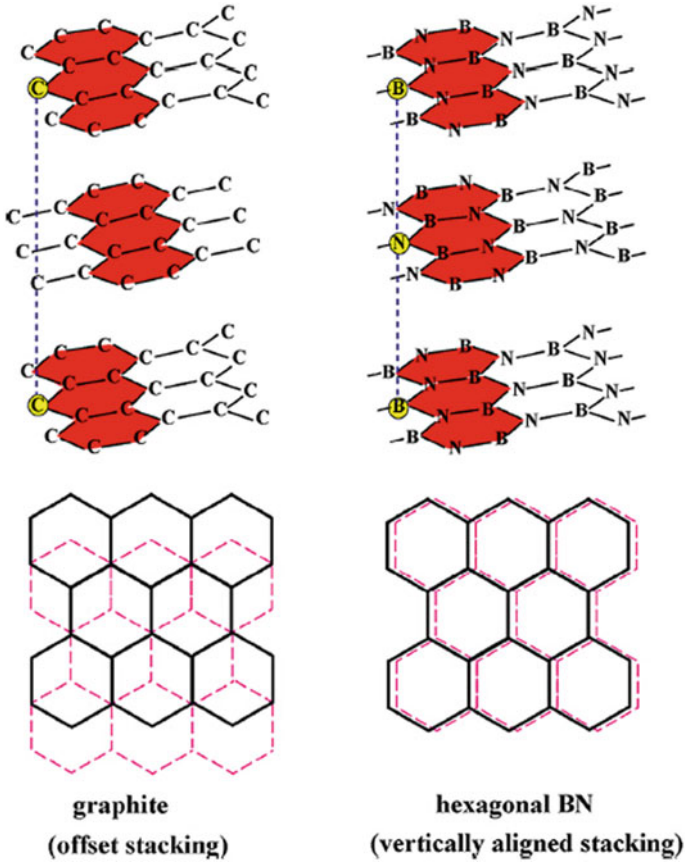


**Fig. 1.18** Structures of graphite and *h*-BN. Reproduced with permission from Ref. [100], © 2013 Elsevier Ltd

excellent thermal conductivity and mechanical strength, good optical properties than graphene, and better chemical and thermal stability.

With a similar lattice constant to graphene and the same hexagonal structure, *h*-BN layers, as ideal planar insulating substrates, offer one of most advanced platforms for graphene-based electronics by enhancing the stability, quality and carrier mobility of graphene [102]. For example, *h*-BN sheets can be used as good back-gate dielectric layer materials for graphene-based field-effect transistors. Because of their commensurate structural parameters and distinct electronic properties, layered heterostructures consisting of graphene and *h*-BN layers have recently attracted intense interests. Stacking these layers in a precisely controlled sequence can give rise to new phenomena and create tailored properties [103, 104].

Aside from *h*-BN, many other 2D materials have also earned tremendous attention, such as graphene derivate (e.g. hydrogenated graphene, fluorinated graphene), layered group-IV and group-III metal chalcogenides (e.g. SnX (X = S, Se, or Te)),

layered oxides and hydroxides (e.g. $V_2O_5$, ZnO). The investigations into these novel materials will generate fantastic properties and amazing applications.

## 1.5 Van der Waals Heterostructures

From the above sections, we can see that since the discovery of the exotic properties of graphene, graphene-like 2D materials have gained widespread attention due to their unique properties that could have many fundamental applications. The ideas and methodology developed in preparing graphene, such as mechanical peeling, molecular beam epitaxial and chemical vapor deposition, have been extended to the exploration of other 2D materials, including some artificially synthesized atomic crystals that do not exist in nature. Moreover, we can tune the structures and electronic properties of these two-dimensional materials by various methods, such as chemical or molecular doping, atomic or molecular intercalation, and exertion of tension or pressure. It is not difficult to imagine that we can pile up these 2D layers in a controlled manner to form new 3D stacked materials, as shown in Fig. 1.19. Given that each individual component exhibits distinct properties, we possess a library of 2D atomic crystals, which allows us to create 3D layered structures with novel and tailored properties, with an ultimate desire for a vast library containing various functional materials. This is the basic principle of van der Waals heterostructures techniques, a growing research field in the past years [24, 105]. This approach involves three

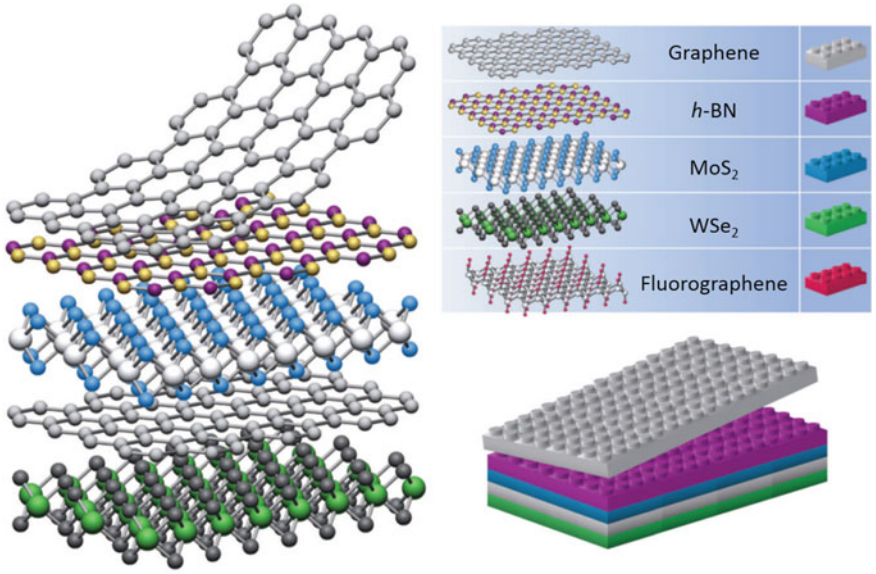


**Fig. 1.19** Van der Waals heterostructures. Reprinted from Ref. [24], © 2013 Springer Nature

processes: (a) preparing various 2D materials by mechanical exfoliation and/or synthetic growth; (b) tuning electronic, optical and chemical properties of these 2D materials by chemical modification or applying stress or external field; (c) stacking these 2D crystals on top of each other in a controlled fashion to generate new hybrid structures. The development of these novel heterostructures paves a way towards a variety of practical applications since it could create artificial materials that exhibit unique properties and multiple functions.

## 1.6 Research Contents and Instruments

### *1.6.1 Research Contents*

The successful exfoliation of graphene out of graphite resulted in the first real two-dimensional material in nature. Its unique electronic structures and exotic properties were subsequently revealed, followed by fruitful results of graphene-related fundamental researches and practical applications. Graphene is undoubtedly the most dazzling research focus in the field of material science in the past decade. More importantly, graphene opens up, or at least reactivates the research field of 2D materials, and arouses researchers' enthusiasm for the exploration of 2D materials. A focused effort on growth and isolation of high-quality single-layer nanosheets was re-initiated after the discovery of graphene, including some two-dimensional systems that have been studied in the past and re-examined now from a new perspective. In this context, the research in this thesis was performed on graphene-like 2D crystal materials, focusing mainly on germanene, hafnium honeycomb crystal, and platinum diselenide. The preparation methods, atomic structures, electronic properties as well as practical applications of the above materials were studied systematically.

The thesis contains five parts and is ordered as follows. Following this introduction part, Chap. 2 presents the growth method of single-layer germanene and reveals its superstructures on the metal substrate by means of experimental characterizations and theoretical calculations. In Chap. 3, the fabrication of honeycomb-like structures based on the transition metal element is reported for the first time. Atomically-resolved STM images show that hafnium atoms form a long-range ordered honeycomb structure on an Ir (111) substrate. The calculated density of states and STM simulation confirm that Hf atoms are assembled into a continuous 2D honeycomb lattice through covalent bonding. Chap. 4 involves another type of 2D layered materials beyond graphene-transition metal dichalcogenides (TMDs). We report on the preparation of a new TMD, monolayer platinum diselenide ($PtSe_2$) on a Pt(111) surface, by a brand new synthesis strategy. A variety of surface characterization methods have revealed the atomic structure and interfacial characteristics of single-layer $PtSe_2$. Angle-resolved photoemission spectroscopy (ARPES) demonstrates its semiconducting features. Besides, we have carried out photocatalytic investigations

and predicted the application in valley electronics theoretically. Lastly, the thesis ends in the 5th chapter with important conclusions and prospect of the work.

### *1.6.2 Introduction of Instruments*

Most of the experiments involved in this thesis were performed on the ultra-high vacuum (UHV) chambers equipped with a commercial variable-temperature scanning tunneling microscope (Omicron VT-STM), as shown in Fig. 1.20. The system contains a preparation chamber, an analysis chamber, a load-lock chamber for rapid sample transmission and other ancillary facilities. The preparation chamber is the largest chamber, which includes many instruments for substrate cleaning, sample preparation, and experimental characterization, such as Ar ion sputtering gun, low-energy electron diffraction (LEED), electron-beam heating stage (EBH), and molecular beam epitaxy (MBE) evaporators. All the single crystals are cleaned by several cycles of sputtering with the Ar ion sputtering gun and annealing on the EBH. The clean and flat metal surfaces serve as the epitaxial substrates for growth of 2D materials. The growth process and the structural properties are controlled using the EBH by accurate control over the growth temperature. LEED is used for the determination of the surface structure and symmetry of 2D atomic crystals. The leakage valves connected to various external gases provide a precisely controllable gas pressure for the synthesis of 2D films. These instruments and facilities on the preparation chamber ensure the controllable fabrication of 2D crystalline materials. In addition, the preparation chamber is connected to a small load-lock chamber, which allows us to load and transfer samples from the atmosphere in a fast manner without breaking the vacuum of the preparation chamber. The core part of the whole system is the VT-STM in the analysis chamber. It can obtain atomic-resolution topographic and

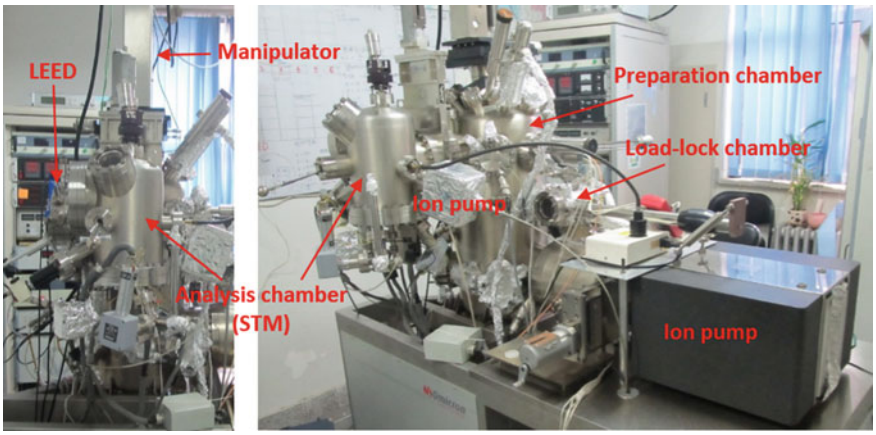


**Fig. 1.20** UHV-MBE-VTSTM system

electronic characteristics, which is the chief approach of in situ characterization of sample quality and surface structure. The ancillary facilities include ultra-high vacuum pumps, vibration isolation systems, home-made gas lines, gas station, and so on.

Other characterization techniques, such as scanning transmission electron microscope (STEM), angle-resolved photoemission spectroscopy (ARPES), Raman spectroscopy, and X-ray photoelectron spectroscopy (XPS) were performed in our cooperative groups or public experimental platforms. A home-made sample delivery chamber is used to transfer samples between our chamber and other cooperative UHV systems, in which a UHV environment of $10^{-10}$ mbar is maintained at all time during sample delivery.

## References

1. Novoselov KS et al (2004) Electric field effect in atomically thin carbon films. Science 306:666–669. https://doi.org/10.1126/science.1102896
2. Geim AK, Novoselov KS (2007) The rise of graphene. Nat Mater 6:183–191
3. Neto AHC, Guinea F, Peres NMR, Novoselov KS, Geim AK (2009) The electronic properties of graphene. Rev Mod Phys 81:109–154
4. Zhang YB, Tan YW, Stormer HL, Kim P (2005) Experimental observation of the quantum Hall effect and Berry's phase in graphene. Nature 438:201–204. https://doi.org/10.1038/nature04235
5. Jiang Z, Zhang Y, Tan YW, Stormer HL, Kim P (2007) Quantum Hall effect in graphene. Solid State Commun 143:14–19. https://doi.org/10.1016/j.ssc.2007.02.046
6. Novoselov KS et al (2007) Room-temperature quantum hall effect in graphene. Science 315:1379. https://doi.org/10.1126/science.1137201
7. Balandin AA et al (2008) Superior thermal conductivity of single-layer graphene. Nano Lett 8:902–907. https://doi.org/10.1021/nl0731872
8. Lee C, Wei X, Kysar JW, Hone J (2008) Measurement of the elastic properties and intrinsic strength of monolayer graphene. Science 321:385–388. https://doi.org/10.1126/science.1157996
9. Nair RR et al (2008) Fine structure constant defines visual transparency of graphene. Science 320:1308. https://doi.org/10.1126/science.1156965
10. Schedin F et al (2007) Detection of individual gas molecules adsorbed on graphene. Nat Mater 6:652–655. https://doi.org/10.1038/nmat1967
11. Lin YM et al (2010) 100-GHz transistors from wafer-scale epitaxial graphene. Science 327:662. https://doi.org/10.1126/science.1184289
12. Kim K, Choi J-Y, Kim T, Cho S-H, Chung H-J (2011) A role for graphene in silicon-based semiconductor devices. Nature 479:338–344
13. Lin Y-M et al (2011) Wafer-scale graphene integrated circuit. Science 332:1294–1297. https://doi.org/10.1126/science.1204428
14. Novoselov KS et al (2012) A roadmap for graphene. Nature 490:192–200. https://doi.org/10.1038/nature11458
15. Coraux J et al (2009) Growth of graphene on Ir(111). New J Phys 11:023006. https://doi.org/10.1088/1367-2630/11/2/023006
16. Emtsev KV et al (2009) Towards wafer-size graphene layers by atmospheric pressure graphitization of silicon carbide. Nat Mater 8:203–207. https://doi.org/10.1038/nmat2382
17. Juang Z-Y et al (2009) Synthesis of graphene on silicon carbide substrates at low temperature. Carbon 47:2026–2031. https://doi.org/10.1016/j.carbon.2009.03.051

18. Pan Y et al (2009) Highly ordered, millimeter-scale, continuous, single-crystalline graphene monolayer formed on Ru(0001). Adv Mater 21:2777. https://doi.org/10.1002/adma.200800761
19. Sutter P, Sadowski JT, Sutter E (2009) Graphene on Pt(111): growth and substrate interaction. Phys Rev B 80:245411. https://doi.org/10.1103/PhysRevB.80.245411
20. Bae S et al (2010) Roll-to-roll production of 30-inch graphene films for transparent electrodes. Nat Nanotechnol 5:574–578. https://doi.org/10.1038/nnano.2010.132
21. Murata Y et al (2010) Orientation-dependent work function of graphene on Pd(111). Appl Phys Lett 97:143114. https://doi.org/10.1063/1.3495784
22. Zhu Y et al (2010) Graphene and graphene oxide: synthesis, properties, and applications. Adv Mater 22:3906–3924. https://doi.org/10.1002/adma.201001068
23. Gao M et al (2011) Epitaxial growth and structural property of graphene on Pt(111). Appl Phys Lett 98:033101
24. Geim AK, Grigorieva IV (2013) Van der Waals heterostructures. Nature 499:419–425. https://doi.org/10.1038/nature12385
25. Sipos B et al (2008) From Mott state to superconductivity in 1T-$TaS_2$. Nat Mater 7:960–965. https://doi.org/10.1038/nmat2318
26. Mak KF, Lee C, Hone J, Shan J, Heinz TF (2010) Atomically thin $MoS_2$: a new direct-gap semiconductor. Phys Rev Lett 105:136805
27. Yin Z et al (2011) Single-layer $MoS_2$ phototransistors. ACS Nano 6:74–80
28. Cao T et al (2012) Valley-selective circular dichroism of monolayer molybdenum disulphide. Nat Commun 3:887
29. Mak KF, He K, Shan J, Heinz TF (2012) Control of valley polarization in monolayer $MoS_2$ by optical helicity. Nat Nanotechnol 7:494–498. https://doi.org/10.1038/nnano.2012.96
30. Wang QH, Kalantar-Zadeh K, Kis A, Coleman JN, Strano MS (2012) Electronics and optoelectronics of two-dimensional transition metal dichalcogenides. Nat Nanotechnol 7:699–712. https://doi.org/10.1038/nnano.2012.193
31. Yang JJ et al (2012) Charge-orbital density wave and superconductivity in the strong spin-orbit coupled $IrTe_2$:Pd. Phys Rev Lett 108:116402. https://doi.org/10.1103/PhysRevLett.108.116402
32. Zeng H, Dai J, Yao W, Xiao D, Cui X (2012) Valley polarization in $MoS_2$ monolayers by optical pumping. Nat Nanotechnol 7:490–493. https://doi.org/10.1038/nnano.2012.95
33. Butler SZ et al (2013) Progress, challenges, and opportunities in two-dimensional materials beyond graphene. ACS Nano 7:2898–2926. https://doi.org/10.1021/nn400280c
34. Lebegue S, Bjorkman T, Klintenberg M, Nieminen RM, Eriksson O (2013) Two-dimensional materials from data filtering and ab initio calculations. Phys Rev X 3:031002. https://doi.org/10.1103/PhysRevX.3.031002
35. Najmaei S et al (2013) Vapour phase growth and grain boundary structure of molybdenum disulphide atomic layers. Nat Mater 12:754–759. https://doi.org/10.1038/nmat3673
36. Rao CNR, Matte HSSR, Maitra U (2013) Graphene analogues of inorganic layered materials. Angewe Chem Int Ed 52:13162–13185. https://doi.org/10.1002/anie.201301548
37. van der Zande AM et al (2013) Grains and grain boundaries in highly crystalline monolayer molybdenum disulphide. Nat Mater 12:554–561. https://doi.org/10.1038/nmat3633
38. Xu MS, Liang T, Shi MM, Chen HZ (2013) Graphene-like two-dimensional materials. Chem Rev 113:3766–3798. https://doi.org/10.1021/cr300263a
39. Fiori G et al (2014) Electronics based on two-dimensional materials (vol 9, pg 768, 2014). Nat Nanotechnol 9:1063. https://doi.org/10.1038/Nnano.2014.283
40. Koppens FHL et al (2014) Photodetectors based on graphene, other two-dimensional materials and hybrid systems. Nat Nanotechnol 9:780–793. https://doi.org/10.1038/Nnano.2014.215
41. Mak KF, McGill KL, Park J, McEuen PL (2014) The valley Hall effect in $MoS_2$ transistors. Science 344:1489–1492. https://doi.org/10.1126/science.1250140
42. Xu XD, Yao W, Xiao D, Heinz TF (2014) Spin and pseudospins in layered transition metal dichalcogenides. Nat Phys 10:343–350. https://doi.org/10.1038/Nphys2942

43. Sie EJ et al (2015) Valley-selective optical Stark effect in monolayer $WS_2$. Nat Mater 14:290–294
44. Helveg S et al (2000) Atomic-scale structure of single-layer $MoS_2$ nanoclusters. Phys Rev Lett 84:951–954. https://doi.org/10.1103/PhysRevLett.84.951
45. Rao CNR, Nag A (2010) Inorganic analogues of graphene. Eur J Inorg Chem 4244–4250:2010. https://doi.org/10.1002/ejic.201000408
46. Zhu ZY, Cheng YC, Schwingenschlogl U (2011) Giant spin-orbit-induced spin splitting in two-dimensional transition-metal dichalcogenide semiconductors. Phys Rev B 84:153402. https://doi.org/10.1103/PhysRevB.84.153402
47. Liu C-C, Feng W, Yao Y (2011) Quantum spin hall effect in silicene and two-dimensional germanium. Phys Rev Lett 107:076802
48. Chen L et al (2012) Evidence for dirac fermions in a honeycomb lattice based on silicon. Phys Rev Lett 109:056804
49. Feng B et al (2012) Evidence of silicene in honeycomb structures of silicon on Ag(111). Nano Lett 12:3507–3511. https://doi.org/10.1021/nl301047g
50. Fleurence A et al (2012) Experimental evidence for epitaxial silicene on diboride thin films. Phys Rev Lett 108:245501. https://doi.org/10.1103/PhysRevLett.108.245501
51. Gao J, Zhao J (2012) Initial geometries, interaction mechanism and high stability of silicene on Ag(111) surface. Sci Rep 2:861. https://doi.org/10.1038/srep00861
52. Vogt P et al (2012) Silicene: compelling experimental evidence for graphenelike two-dimensional silicon. Phys Rev Lett 108:155501. https://doi.org/10.1103/PhysRevLett.108.155501
53. Meng L et al (2013) Buckled silicene formation on Ir(111). Nano Lett 13:685–690. https://doi.org/10.1021/nl304347w
54. Li L et al (2014) Buckled germanene formation on Pt(111). Adv Mater 26:4820–4824. https://doi.org/10.1002/adma.201400909
55. Splendiani A et al (2010) Emerging photoluminescence in monolayer $MoS_2$. Nano Lett 10:1271–1275. https://doi.org/10.1021/nl903868w
56. Eda G et al (2011) Photoluminescence from chemically exfoliated $MoS_2$. Nano Lett 11:5111–5116. https://doi.org/10.1021/nl201874w
57. Radisavljevic B, Radenovic A, Brivio J, Giacometti V, Kis A (2011) Single-layer $MoS_2$ transistors. Nat Nanotechnol 6:147–150
58. Chhowalla M et al (2013) The chemistry of two-dimensional layered transition metal dichalcogenide nanosheets. Nat Chem 5:263–275. https://doi.org/10.1038/nchem.1589
59. Li LK et al (2014) Black phosphorus field-effect transistors. Nat Nanotechnol 9:372–377. https://doi.org/10.1038/Nnano.2014.35
60. Tao L et al (2015) Silicene field-effect transistors operating at room temperature. Nat Nanotechnol 10:227–231. https://doi.org/10.1038/nnano.2014.325
61. Novoselov K et al (2005) Two-dimensional atomic crystals. Proc Natl Acad Sci U S A 102:10451–10453
62. Coleman JN et al (2011) Two-dimensional nanosheets produced by liquid exfoliation of layered materials. Science 331:568–571
63. Nicolosi V, Chhowalla M, Kanatzidis MG, Strano MS, Coleman JN (2013) Liquid exfoliation of layered materials. Science 340:1226419
64. Li X et al (2011) Large-area graphene single crystals grown by low-pressure chemical vapor deposition of methane on copper. J Am Chem Soc 133:2816–2819. https://doi.org/10.1021/ja109793s
65. Liu K-K et al (2012) Growth of large-area and highly crystalline $MoS_2$ thin layers on insulating substrates. Nano Lett 12:1538–1544. https://doi.org/10.1021/nl2043612
66. Zhan Y, Liu Z, Najmaei S, Ajayan PM, Lou J (2012) Large-area vapor-phase growth and characterization of $MoS_2$ atomic layers on a $SiO_2$ substrate. Small 8:966–971. https://doi.org/10.1002/smll.201102654
67. Lee Y-H et al (2013) Synthesis and transfer of single-layer transition metal disulfides on diverse surfaces. Nano Lett 13:1852–1857. https://doi.org/10.1021/nl400687n

68. Lu X et al (2014) Large-area synthesis of monolayer and few-layer $MoSe_2$ films on $SiO_2$ substrates. Nano Lett 14:2419–2425. https://doi.org/10.1021/nl5000906
69. Takeda K, Shiraishi K (1994) Theoretical possibility of stage corrugation in Si and Ge analogs of graphite. Phys Rev B 50:14916–14922
70. Cahangirov S, Topsakal M, Aktürk E, Şahin H, Ciraci S (2009) Two- and one-dimensional honeycomb structures of silicon and germanium. Phys Rev Lett 102:236804
71. Aufray B et al (2010) Graphene-like silicon nanoribbons on Ag(110): a possible formation of silicene. Appl Phys Lett 96:183102. https://doi.org/10.1063/1.3419932
72. De Padova P et al (2010) Evidence of graphene-like electronic signature in silicene nanoribbons. Appl Phys Lett 96:261905
73. Tchalala MR et al (2014) Atomic structure of silicene nanoribbons on Ag (110). J Phys Conf Ser 491:012002
74. Lalmi B et al (2010) Epitaxial growth of a silicene sheet. Appl Phys Lett 97:223109
75. Le Lay G, De Padova P, Resta A, Bruhn T, Vogt P (2012) Epitaxial silicene: can it be strongly strained? J Phys D Appl Phys 45:392001
76. Lin C-L et al (2012) Structure of silicene grown on Ag(111). Appl Phys Express 5:045802. https://doi.org/10.1143/apex.5.045802
77. Jamgotchian H et al (2012) Growth of silicene layers on Ag (111): unexpected effect of the substrate temperature. J Phys Condens Matter 24:172001
78. Kuc A, Zibouche N, Heine T (2011) Influence of quantum confinement on the electronic structure of the transition metal sulfide $TS_2$. Phys Rev B 83:245213. https://doi.org/10.1103/PhysRevB.83.245213
79. Zhang Y et al (2014) Direct observation of the transition from indirect to direct bandgap in atomically thin epitaxial $MoSe_2$. Nat Nanotechnol 9:111–115. https://doi.org/10.1038/Nnano.2013.277
80. Novoselov K (2011) Nobel lecture: graphene: materials in the flatland. Rev Mod Phys 83:837
81. Smith RJ et al (2011) Large-scale exfoliation of inorganic layered compounds in aqueous surfactant solutions. Adv Mater 23:3944–3948
82. Zeng Z et al (2011) Single-Layer Semiconducting Nanosheets: High-Yield Preparation and Device Fabrication. Angew Chem Int Ed 50:11093–11097. https://doi.org/10.1002/anie.201106004
83. Cunningham G et al (2012) Solvent exfoliation of transition metal dichalcogenides: dispersibility of exfoliated nanosheets varies only weakly between compounds. ACS Nano 6:3468–3480
84. Zeng Z et al (2012) An effective method for the fabrication of few-layer-thick inorganic nanosheets. Angew Chem Int Ed 51:9052–9056. https://doi.org/10.1002/anie.201204208
85. Lee YH et al (2012) Synthesis of large-area $MoS_2$ atomic layers with chemical vapor deposition. Adv Mater 24:2320–2325
86. Shi Y et al (2012) Van der Waals epitaxy of $MoS_2$ layers using graphene as growth templates. Nano Lett 12:2784–2791
87. Peng Y et al (2001) Hydrothermal synthesis and characterization of single-molecular-layer $MoS_2$ and $MoSe_2$. Chem Lett 30:772–773
88. Peng Y et al (2001) Hydrothermal synthesis of $MoS_2$ and its pressure-related crystallization. J Solid State Chem 159:170–173
89. Ramakrishna Matte H et al (2010) $MoS_2$ and $WS_2$ analogues of graphene. Angew Chem 122:4153–4156
90. RamakrishnaáMatte H (2011) Graphene analogues of layered metal selenides. Dalton Trans 40:10322–10325
91. Schwierz F (2010) Graphene transistors. Nat Nanotechnol 5:487–496
92. Wu Y et al (2011) High-frequency, scaled graphene transistors on diamond-like carbon. Nature 472:74–78
93. Wu Y et al (2012) State-of-the-art graphene high-frequency electronics. Nano Lett 12:3062–3067
94. Colinge J-P (2004) Multiple-gate soi mosfets. Solid-State Electron 48:897–905

95. Yoon Y, Ganapathi K, Salahuddin S (2011) How good can monolayer $MoS_2$ transistors be? Nano Lett 11:3768–3773
96. Polman A, Atwater HA (2012) Photonic design principles for ultrahigh-efficiency photovoltaics. Nat Mater 11:174–177
97. Carladous A et al (2002) Light emission from spectral analysis of Au/$MoS_2$ nanocontacts stimulated by scanning tunneling microscopy. Phys Rev B 66:045401
98. Kirmayer S, Aharon E, Dovgolevsky E, Kalina M, Frey GL (2007) Self-assembled lamellar $MoS_2$, $SnS_2$ and $SiO_2$ semiconducting polymer nanocomposites. Philos Trans R Soc A: Math Phys Eng Sci 365:1489–1508
99. Zeng H et al (2010) "White graphenes": boron nitride nanoribbons via boron nitride nanotube unwrapping. Nano Lett 10:5049–5055
100. Tang Q, Zhou Z (2013) Graphene-analogous low-dimensional materials. Prog Mater Sci 58:1244–1315
101. Kubota Y, Watanabe K, Tsuda O, Taniguchi T (2007) Deep ultraviolet light-emitting hexagonal boron nitride synthesized at atmospheric pressure. Science 317:932–934
102. Yang W et al (2013) Epitaxial growth of single-domain graphene on hexagonal boron nitride. Nat Mater 12:792–797
103. Dean C et al (2010) Boron nitride substrates for high-quality graphene electronics. Nat Nanotechnol 5:722–726
104. Ponomarenko L et al (2011) Tunable metal-insulator transition in double-layer graphene heterostructures. Nat Phys 7:958–961
105. Niu TC, Li A (2015) From two-dimensional materials to heterostructures. Prog Surf Sci 90:21–45. https://doi.org/10.1016/j.progsurf.2014.11.001